Check for updates

Biochemical Journal (2018) **475** 1335–1352
https://doi.org/10.1042/BCJ20180070

PORTLAND PRESS

Research Article

Pre-equilibrium competitive library screening for tuning inhibitor association rate and specificity toward serine proteases

Itay Cohen[1], Si Naftaly[1], Efrat Ben-Zeev[2], Alexandra Hockla[3], Evette S. Radisky[3] and Niv Papo[1]

[1]Department of Biotechnology Engineering and the National Institute of Biotechnology in the Negev, Ben-Gurion University of the Negev, Beer-Sheva, Israel; [2]The Nancy and Stephen Grand Israel National Center for Personalized Medicine, Weizmann Institute of Science, Rehovot, Israel; [3]Department of Cancer Biology, Mayo Clinic Comprehensive Cancer Center, Jacksonville, FL, U.S.A.

Correspondence: Niv Papo (papo@bgu.ac.il)

High structural and sequence similarity within protein families can pose significant challenges to the development of selective inhibitors, especially toward proteolytic enzymes. Such enzymes usually belong to large families of closely similar proteases and may also hydrolyze, with different rates, protein- or peptide-based inhibitors. To address this challenge, we employed a combinatorial yeast surface display library approach complemented with a novel pre-equilibrium, competitive screening strategy for facile assessment of the effects of multiple mutations on inhibitor association rates and binding specificity. As a proof of principle for this combined approach, we utilized this strategy to alter inhibitor/protease association rates and to tailor the selectivity of the amyloid β-protein precursor Kunitz protease inhibitor domain (APPI) for inhibition of the oncogenic protease mesotrypsin, in the presence of three competing serine proteases, anionic trypsin, cationic trypsin and kallikrein-6. We generated a variant, designated $APPI_{P13W/M17G/I18F/F34V}$, with up to 30-fold greater specificity relative to the parental $APPI_{M17G/I18F/F34V}$ protein, and 6500- to 230 000-fold improved specificity relative to the wild-type APPI protein in the presence of the other proteases tested. A series of molecular docking simulations suggested a mechanism of interaction that supported the biochemical results. These simulations predicted that the selectivity and specificity are affected by the interaction of the mutated APPI residues with nonconserved enzyme residues located in or near the binding site. Our strategy will facilitate a better understanding of the binding landscape of multispecific proteins and will pave the way for design of new drugs and diagnostic tools targeting proteases and other proteins.

Introduction

Extracellular proteases that are aberrantly expressed in the tumor microenvironment are key contributors to cancer growth, progression and metastasis [1–3] and hence constitute a promising category of drug targets [4,5]. Although the potential of targeting these extracellular proteases was recognized some years ago, it remains unrealized, whereas for other extracellular drug targets, including cell surface receptors and soluble signaling factors, the past two decades have seen the emergence of many successful protein-based therapeutics. Most of these therapeutics are based on monoclonal antibodies [6,7], which exert their biological activities either through immune-related effector functions or by inhibiting dysregulated ligand–receptor interactions. A key advantage of this type of targeting through protein–protein interactions is that the selectivity of the targeting agents is far narrower than that of small molecule drugs, resulting in low off-target toxicity. This selectivity advantage of protein

Received: 24 January 2018
Revised: 9 March 2018
Accepted: 12 March 2018

Accepted Manuscript online: 13 March 2018
Version of Record published: 16 April 2018

© 2018 The Author(s). Published by Portland Press Limited on behalf of the Biochemical Society

Downloaded from http://portlandpress.com/biochemj/article-pdf/475/7/1335/694517/bcj-2018-0070.pdf by Ben-Gurion University of the Negev user on 23 August 2021

Biochemical Journal (2018) 475 1335–1352
https://doi.org/10.1042/BCJ20180070

therapeutics (namely, enzyme inhibitors) is particularly critical for the development of drugs targeting oncogenic proteases, since the target enzymes belong to large families of closely related molecules, some of which perform key biological functions or serve protective roles in the context of cancer [8].

As an integral part of inhibitor-/protease-binding affinity and specificity, the concentrations of both the inhibitor and the protease — as reflected by the second-order rate constant of target association (k_{on}, see below) — are crucial for effective targeting *in vivo*, since they control the rate of the interaction. The biological effect of the inhibitor is, in turn, strongly influenced by the rate of the interaction, since many *in vivo* processes are not in equilibrium. Indeed, it has been shown that fast target association can increase the local (e.g. tumor) concentration of the drug, which impedes the rate of decline in target occupancy [9]. In the case of cancers, increased inhibitor concentration near the tumor as a result of rapid association with the target may also lead to better local specificity, that is, less drug will be available to other regions/organs of the patient, and thus, there will be a reduction in off-target toxicity. Thus, to achieve effective selectivity *in vivo*, not only high affinity but also rapid association to cancer-related proteases, in preference to other competing proteases, is required.

In this study, we used combinatorial methods, guided by structure-based insights obtained from our recently solved prototype inhibitor/protease complex [10], to develop a new class of nonimmunoglobulin-based protein scaffolds that rapidly (high k_{on} rates) and selectively target mesotrypsin, an oncogenic protease that plays key roles in cancer progression and metastasis. Human mesotrypsin, which is encoded by the *PRSS3* gene, belongs to the chymotrypsin superfamily of serine endopeptidases. This enzyme, which cleaves peptide bonds of specific substrates on the carboxyl side of Arg or Lys at pH ~8.0 [11], is normally expressed in low levels in the pancreas, as a digestive trypsin, and in the brain, where it has no known function. Many studies have shown that up-regulation of mesotrypsin by cancer cells and tumors is associated with increased malignancy and that mesotrypsin functionally drives multiple aspects of the malignant progression of lung, pancreas, prostate and breast cancers [12–15]. In pancreatic cancer, mesotrypsin expression was correlated with metastasis and the associated poor patient survival [15]. In cell culture and xenograft models of pancreatic cancer, overexpression of mesotrypsin promoted invasion, proliferation and growth of larger tumors, while suppression of mesotrypsin expression reduced cell growth and invasion and delayed progression to metastasis [15]. Hockla et al. [13] found high expression of mesotrypsin in primary prostate tumors to be prognostic for early cancer recurrence following prostatectomy. Using an orthotopic model of metastatic prostate cancer, we demonstrated that silencing of mesotrypsin in cancer cells led to slower tumor growth and greatly reduced metastasis, while in cell culture models, mesotrypsin silencing reduced invasion and anchorage-independent growth [13]. Notably, while treatment with the active form of recombinant mesotrypsin directly promoted an invasive cellular phenotype in prostate cancer cells, neither cationic trypsin nor a noncatalytic mesotrypsin variant could similarly drive this invasive phenotype, suggesting that these effects were dependent on the specific proteolytic activity of mesotrypsin [13]. The above studies suggest that mesotrypsin may constitute a promising target for antimetastatic therapy if selective inhibitors can be identified.

To date, no specific inhibitors against mesotrypsin, either natural or synthetic, have been reported, probably because targeting mesotrypsin presents two distinct challenges: (i) not only is mesotrypsin resistant to inhibition by many polypeptide serine protease inhibitors [11,16,17], but it also possesses enhanced catalytic capability for their hydrolysis [18–22] and (ii) mesotrypsin has a close structural relationship with other trypsin-like proteases, making it difficult to achieve specific targeting. However, X-ray crystallography studies by our group and others have identified four unique active-site features that distinguish mesotrypsin from other serine proteases [16,19,22]. Most notable are two adaptive mutations that are absent from other serine proteases, namely, G193R, which clashes sterically with trypsin inhibitors, and Y39S, which prevents the formation of hydrogen bonds within mesotrypsin/inhibitor complexes. Although it has been found that these mutations confer on mesotrypsin low affinity for polypeptide trypsin inhibitors and that they contribute to the ability of mesotrypsin to cleave canonical trypsin inhibitors at an accelerated rate [19,22,23], similar and even greater effects were observed for these two mutations working together with the other two unique mesotrypsin residues, namely, Lys-74 with Arg-193 and Asp-97 with Ser-39 [22]. The overall effect of these four residues is the weakening of favorable (strong) interactions, the promotion of unfavorable (weak) interactions and the enhancement of protein dynamics at the mesotrypsin-/inhibitor-binding interface. By taking advantage of such unique features that distinguish mesotrypsin from related enzymes, we aimed to develop novel selective inhibitors that would overcome the resistance of mesotrypsin to inhibition.

Our approach to developing rapidly associating, selective mesotrypsin inhibitors employed combinatorial engineering based on the scaffold of the human amyloid β-protein precursor Kunitz protease inhibitor domain

Downloaded from http://portlandpress.com/biochemj/article-pdf/475/7/1335/694517/bcj-2018-0070.pdf by Ben-Gurion University of the Negev user on 23 August 2021

© 2018 The Author(s). Published by Portland Press Limited on behalf of the Biochemical Society

Biochemical Journal (2018) 475 1335–1352
https://doi.org/10.1042/BCJ20180070

PORTLAND PRESS

(APPI), which is a member of the human Kunitz domain family of serine protease inhibitors. This protein attracted our interest as a scaffold for engineering tumor-targeting proteins for several reasons: (i) APPI is a small, compact protein (58 amino acids) that is stabilized by a hydrophobic core and by three disulfide bonds [24], resulting in high thermal stability [10]. (ii) We anticipate that APPI will be nonimmunogenic due to its human source. (iii) There is marked sequence diversity among Kunitz family members, and the canonical binding loops are highly tolerant to substitution or incorporation of additional amino acids [25]. These attributes offer a substantial opportunity to optimize target affinity and selectivity without compromising stability.

Work from the Radisky laboratory showed that native APPI possesses a relatively low affinity [inhibition constant (K_i) of 140 nM] for mesotrypsin and is susceptible to cleavage and inactivation by this enzyme [20]. It was also found that mesotrypsin affinity and specificity are largely directed by the sequence of the canonical binding loop, while proteolytic stability is influenced by both binding loop residues and residues that are buried within the inhibitor scaffold [10,24,26,27]. In light of these results, we have previously attempted to simultaneously optimize the affinity and proteolytic stability of APPI by using combinatorial screening methods as a means to generate selective APPI-based mesotrypsin inhibitors with increased proteolytic stability and stronger binding affinity [10]. In that study, we demonstrated that the APPI protein scaffold is indeed suitable for optimization using the yeast surface display (YSD) platform [10], a powerful directed evolution technology for engineering proteins [28–33]. With that strategy, we generated a triple APPI mutant with enhanced affinity for mesotrypsin and superior resistance to cleavage versus wild-type APPI [10], thereby overcoming the resistance of mesotrypsin to inhibition. We found that the triple mutant inhibited mesotrypsin-dependent cancer cell growth, invasion and migration of PC3-M prostate cancer cells, although these inhibitory effects were not as pronounced as those for mesotrypsin knockdown, presumably as a result of the limited selectivity of this inhibitor. The need for a major enhancement of the selectivity of the APPI triple mutant was therefore the rationale for conducting the current study.

Here, we constructed a combinatorial library of APPI mutants that was rich in mutations enhancing stability, affinity, specificity and rapid association. By using this YSD APPI library to conduct selective screens under pre-equilibrium conditions of mesotrypsin competition versus other human serine proteases, we identified high-affinity, highly resistant and highly selective mesotrypsin-targeting protein inhibitors with an improved association rate with potential for clinical translation as imaging and therapeutic agents. These novel inhibitors will serve as extremely valuable laboratory reagents for deciphering the specific mechanisms by which mesotrypsin drives cancer progression and for understanding the basis of target specificity and proteolytic resistance of inhibitors to proteolytic enzymes in general and serine proteases in particular.

Materials and methods

Reagents and additional methods are described in Supplementary Materials and Methods.

Generation of a combinatorial APPI library

An APPI library, which was constructed on the basis of our previously published $APPI_{M17G/I18F/F34V}$ sequence [10], was cloned into the YSD vector as described in detail in Supplementary Materials and Methods. In brief, the APPI library was generated by error-prone PCR and PCR-assembly protocols using a total of 10 overlapping oligonucleotides. To generate a more focused library, seven of these oligonucleotides were individually randomized by using NNS degenerate codons at specific positions within the APPI inhibitory-binding loop region (positions 11–18, excluding Cys at position 14; Supplementary Figure S1). The resulting gene was amplified and transformed into yeast through homologous recombination, as previously described [34]. The combined mutagenesis strategies (NNS and error prone) generated an average mutagenesis rate of 1–2 amino acid mutations per overall 56 residues of APPI, yielding an experimental library of $\sim 3.5 \times 10^6$ clones.

Flow cytometry analysis and cell sorting

Yeast cells displaying the APPI library or individual APPI clones were grown in an SDCAA selective medium (as for SDCAA plates, but without agar; see Supplementary Materials and Methods) and induced for APPI protein expression with a galactose-containing medium (as for SDCAA, but with galactose instead of dextrose), as recently described [10]. In light of the potential for trypsin autoproteolytic degradation and the potential for degradation of APPI by mesotrypsin, catalytically inactive forms of human anionic trypsin, cationic trypsin and mesotrypsin (each having an S195A mutation) — all fluorescently labeled — were used to detect binding to displayed APPI in flow cytometry and FACS (fluorescence-activated cell sorting) experiments. Owing to low

Downloaded from http://portlandpress.com/biochemj/article-pdf/475/7/1335/694517/bcj-2018-0070.pdf by Ben-Gurion University of the Negev user on 23 August 2021

© 2018 The Author(s). Published by Portland Press Limited on behalf of the Biochemical Society

Biochemical Journal (2018) 475 1335–1352
https://doi.org/10.1042/BCJ20180070

protein yields of recombinant catalytically inactive kallikrein-6_{S195A}, fluorescently labeled active kallikrein-6 (hK6) was used in YSD experiments. APPI expression and binding to individual proteases were detected by incubating $\sim 1 \times 10^6$ yeast cells with a 1 : 50 dilution of mouse anti-c-Myc antibody and different concentrations (0.1–1000 nM, Figure 1) of the respective fluorescently labeled enzyme in trypsin buffer (TB; 100 mM Tris–HCl, pH 8.0, 1 mM $CaCl_2$) supplemented with 1% bovine serum albumin (BSA) for 1 h at room temperature. Thereafter, cells were washed with ice-cold TB, followed by incubation with a 1 : 50 dilution of phycoerythrin-conjugated antimouse secondary antibody for 30 min on ice. Finally, the cells were washed with ice-cold TB, and the fluorescence intensity was analyzed by dual-color flow cytometry (Accuri C6; BD Biosciences). All proteases were labeled with DyLight 650 fluorophore, except mesotrypsin, which was labeled with DyLight 488 dye.

For the selective yeast cell assays (including sorts), $\sim 1 \times 10^6$ of yeast cells were labeled with a mixture of the fluorescently labeled proteases in TB supplemented with 1% BSA for 1 h at room temperature. Then, the cells were washed with ice-cold TB, and cells were analyzed by dual-color flow cytometry (Accuri C6; BD Biosciences) or sorted by FACSAria [Ilse Katz Institute for Nanoscale Science and Technology (IKI), Ben-Gurion University of the Negev (BGU)] as described in Figure 2A,B. In the first sort round (S_0 to get S_1), the cells were sorted (in a step termed 'c-Myc clear') for high APPI expression (mainly by removing clones that had stop codons or frame shifts) as described in Supplementary Materials and Methods. Sorted cells were then grown in a selective medium, and several colonies were sequenced [DNA Microarray and Sequencing Unit (DMSU), NIBN (National Institute for Biotechnology in the Negev) and BGU]. The approximate percentage of the selective populations that were sorted was 3.4, 0.6, 0.7 and 0.5 to obtain sorts S_2 to S_5, respectively. Following each sort, the number of yeast cells used for the subsequent sorts was at least 10-fold in excess of the number of post-sorted cells. At least 20 clones from each round of sorting were sequenced (Supplementary Figure S2). The concentrations of anionic trypsin, cationic trypsin and hK6 in all the selective assays (including sorts) were 12.5, 4.7 and 7 nM, respectively. The concentrations of mesotrypsin in each sort are shown in Figure 2C.

Production of recombinant enzymes

Recombinant human anionic trypsinogen, human cationic trypsinogen and human mesotrypsinogen and their catalytically inactive forms (S195A mutants) were expressed in *Escherichia coli*, extracted from inclusion bodies, refolded, purified and activated with bovine enteropeptidase, as described in previous work [19,26]. Recombinant pro-hK6 [a gift from the laboratory of Aubry Miller; German Cancer Research Center (DKFZ)] was expressed in a virus/insect Sf21 cell line system, purified by nickel affinity chromatography followed by ion-exchange chromatography and activated with bovine enterokinase. Catalytically inactive mesotrypsin was labeled with a DyLight 488 fluorophore, while hK6, cationic trypsin and anionic trypsin were labeled with a DyLight 650 fluorophore. Labeling was carried out via NHS ester chemistry with 1 : 5 enzyme : dye ratio, according to the manufacturer's instructions. Concentrations of active human trypsins were quantified by active-site titration using a pNPGB substrate [35]. Concentrations of hK6 and inactive S195A mutants of mesotrypsin, cationic trypsin and anionic trypsin were determined by UV–Vis absorbance at 280 nm, with extinction coefficients (ε_{280}) of 34 670, 37 525, 38 890 and 41 535 M^{-1} cm^{-1}, respectively.

Production of APPI variants

All APPI variants were cloned into a pPIC9K vector, transformed, expressed in *Pichia pastoris* (*GS115* strain) and purified by nickel affinity chromatography, followed by size-exclusion chromatography, as described in our recent work [10]. Protein purity was validated by SDS–PAGE on a 20% polyacrylamide gel (Supplementary Figure S3), and the mass was determined with a MALDI-TOF REFLEX-IV (Bruker) mass spectrometer (IKI, BGU; data not shown). Purification yields for all APPI variants were 4–6 mg/1 l of medium.

Generation of inhibition progress curves

The concentrations of human and bovine trypsins were quantified by active-site titration using the pNPGB substrate [35]. Concentrations of hK6 and FXIa were determined by UV–Vis absorbance at 280 nm, with ε_{280} of 34 670 and 214.4×10^3 M^{-1} cm^{-1}, respectively. The concentrations of the chromogenic substrates Z-GPR-pNA and S-2366 were determined in an end-point assay from the change in the absorbance caused by the release of *p*-nitroaniline ($\varepsilon_{410} = 8480$ M^{-1} cm^{-1}). The concentration of the fluorogenic substrate BOC-Phe–Ser–Arg-AMC was determined by reconstitution of pre-weighed substrate powder in DMSO. The concentrations of APPI

Downloaded from http://portlandpress.com/biochemj/article-pdf/475/7/1335/694517/bcj-2018-0070.pdf by Ben-Gurion University of the Negev user on 23 August 2021

© 2018 The Author(s). Published by Portland Press Limited on behalf of the Biochemical Society

Biochemical Journal (2018) **475** 1335–1352
https://doi.org/10.1042/BCJ20180070

PORTLAND PRESS

variants were determined by titration with pre-titrated bovine trypsin and the substrate L-BAPA, as previously described [19].

Progress curves for human trypsins were generated as we have recently described, with minor changes [10]. Briefly, stock solutions of enzyme, substrate and APPI proteins were prepared at 40× the desired final concentrations (Supplementary Table S1). Assays were performed in 96-well microplates at 37°C as follows: TB buffer (296 μl), Z-GPR-pNA substrate (8 μl) and APPI (8 μl) were mixed and incubated at 37°C for 10 min. Reactions were then initiated by dilution of the enzyme (8 μl) into the pre-equilibrated mixture; the reactions were followed spectroscopically (as the increase in absorbance at 410 nm) in a Synergy2 microplate spectrophotometer (BioTek) for 1–4 h (Supplementary Table S1). Progress curves of human hK6 were generated in the same way, but with kallikrein buffer (KB; 50 mM Tris–HCl, pH 7.3, 100 mM NaCl and 0.2% BSA) instead of TB buffer and with BOC-Phe–Ser–Arg-AMC as the substrate; the reaction was followed by the change in the fluorescent signal (microplate reader set at 355 nm for excitation and 460 nm for emission). Progress curves for FXIa with $APPI_{P13W/M17G/I18F/F34V}$ were obtained in FXIa buffer (FB; 50 mM Tris–HCl, pH 7.6, 150 mM NaCl, 5 mM $CaCl_2$ and 0.1% BSA) with S-2366 as the substrate, as previously described (see Supplementary Materials and Methods).

Progress curves of hK6 for independent determination of k_{off} were obtained in 96-well microplates at 37°C as follows: APPI and hK6, 60 nM each, were mixed and incubated at 37°C for 2 h. The substrate (BOC-Phe–Ser–Arg-AMC) was prepared in KB buffer at a final concentration of 1 mM and incubated at 37°C for 10 min. Reactions were then initiated by dilution of the enzyme–inhibitor mixture (5 μl) by 60× into the pre-equilibrated substrate (295 μl) and followed by the change in the fluorescence signal.

Progress curve analysis

Values of the equilibrium inhibition constant (K_i^{eq}) were calculated using eqn (1) from the steady-state portions of the progress curves (Figure 4A,4B), as described recently [10]. Eqn (1) describes an equilibrium state of reversible competitive inhibition with slow, tight binding behavior, where V_s and V_0 are the steady-state rates in the presence and absence of inhibitor (Figure 4A,4B), K_M is the Michaelis constant for substrate cleavage, and $[S]_0$ and $[I]_0$ are the initial concentrations of substrate and inhibitor, respectively.

$$\frac{(V_0 - V_s)}{V_s} = \frac{[I]_0}{K_i^{eq}(1 + [S]_0/K_M)} \tag{1}$$

Association (k_{on}) and dissociation (k_{off}) constants for slow inhibition of mesotrypsin, anionic trypsin and cationic trypsin were obtained using eqns (2–5) [36]. Data from the generated curves were first globally fitted by multiple regression to eqn (2), with the integrated rate equation describing slow binding inhibition:

$$[P] = \left(\frac{V_0 - V_s}{k_{obs}}\right)\left(1 - e^{-k_{obs}\cdot t}\right) + V_s \cdot t \tag{2}$$

where k_{obs} is the observed first-order rate constant that describes the transition from V_0 to V_s (Figure 4A), and [P] is the concentration of product formed at any time, t.

Slow, tight binding inhibition can be described by two alternative general mechanisms [36]. In brief, one mechanism is a two-step process involving the formation/accumulation of an initial inhibitor–enzyme complex, followed by slow kinetics to form a tighter complex. In this mechanism, k_{on} and k_{off} are both first-order kinetic constants that are characterized by a nonlinear relationship between k_{obs} and the inhibitor concentration. In contrast, the second mechanism is a direct, single-step process in which the final complex is formed slowly. In this mechanism, k_{on} and k_{off} are second- and first-order kinetic constants, respectively, that are characterized by a linear dependence between k_{obs} and the inhibitor concentration [I], as shown in eqn (3). While previous studies of some Kunitz domain inhibitors have found evidence for two-step binding for some inhibitor–protease pairs [37,38], our data were well-fitted by the simpler model, as for all trypsins, a plot of k_{obs} versus inhibitor concentration displayed a linear dependence, consistent with the single-step mechanism (Figure 4C).

$$k_{obs} = k_{off} + \frac{k_{on} \cdot [I]}{1 + [S]_0/K_M} \tag{3}$$

© 2018 The Author(s). Published by Portland Press Limited on behalf of the Biochemical Society

Downloaded from http://portlandpress.com/biochemj/article-pdf/475/7/1335/694517/bcj-2018-0070.pdf by Ben-Gurion University of the Negev user on 23 August 2021

Biochemical Journal (2018) 475 1335–1352
https://doi.org/10.1042/BCJ20180070

k_{on} and k_{off} were calculated from the linear curve generated by eqn (3) and by using the following relationships:

$$k_{on} = \text{slope} \cdot (1 + [S]_0/K_M) \tag{4}$$

$$k_{off} = k_{obs}|_{[I]=0} \tag{5}$$

To validate the correlation between the equilibrium and the kinetic values in our assays, the calculated inhibition constant (K_i^{calc}) was then obtained using eqn (6) and compared with the measuredK_i^{eq}. The results of K_i^{calc} and K_i^{eq} were very similar, with an average deviation error of 15% (Supplementary Tables S2–S4):

$$K_i^{calc} = \frac{k_{off}}{k_{on}} \tag{6}$$

Although APPI inhibitors bound tightly to hK6, the inhibition kinetics was relatively fast; thus, estimation of k_{off} from eqn (3) would be inaccurate. Therefore, k_{off} was calculated independently of the inhibitor concentration by using a multiple regression curve-fit to eqn (7) [36] (Figure 4D).

$$[P] = V_s \cdot t - \frac{V_s}{k_{off}}(1 - e^{-k_{off} \cdot t}) \tag{7}$$

The calculated association rate constant (k_{on}^{calc}) was then obtained from the measured K_i^{eq} by using the following relationship:

$$k_{on}^{calc} = \frac{k_{off}}{K_i^{eq}} \tag{8}$$

Calculations were performed using K_M values of 24.66 ± 1.3 μM for mesotrypsin, 22.84 ± 1.9 μM for cationic trypsin, 10.69 ± 0.65 μM for anionic trypsin and 329.3 ± 2.5 μM for hK6 as determined from at least three Michaelis–Menten kinetic experiments that were recently performed in our laboratory [10]. All curve fittings were done using Prism (GraphPad Software, San Diego, CA). Affinity values (k_{on}, k_{off} and K_i) were used to evaluate improvements in specificity for mesotrypsin vis-à-vis each enzyme by using the following relationships:

$$k_{on}^{specificity} = \left(\frac{k_{on} \text{ for } APPI_{M17G/I18F/F34V} \text{ with Protease X}}{k_{on} \text{ for } APPI_{VARIANT} \text{ with Protease X}}\right) \times \left(\frac{k_{on} \text{ for } APPI_{M17G/I18F/F34V} \text{ with Mesotrypsin}}{k_{on} \text{ for } APPI_{VARIANT} \text{ with Mesotrypsin}}\right)^{-1} \tag{9}$$

$$k^{specificity} = \left(\frac{k \text{ for } APPI_{M17G/I18F/F34V} \text{ with Protease X}}{k \text{ for } APPI_{VARIANT} \text{ with Protease X}}\right)^{-1} \times \left(\frac{k \text{ for } APPI_{M17G/I18F/F34V} \text{with Mesotrypsin}}{k \text{ for } APPI_{VARIANT} \text{ with Mesotrypsin}}\right) \tag{10}$$

where k in eqn (10) can be used for k_{off}, or K_i; $k^{specificity}$reflects the fold affinity changes in mesotrypsin compared with the fold affinity changes in the enzyme of interest (Protease X) upon specific mutation in the APPI sequence. Thus,$k^{specificity} > 1$ means a specificity improvement for mesotrypsin.

The analysis of curves for FXIa with $APPI_{P13W/M17G/I18F/F34V}$ was performed as previously described using Supplementary eqn (S1) from Supplementary Materials and Methods.

Molecular modeling and docking

The mutation of APPI Pro-13 to Trp (P13W) was performed using the Schrödinger Maestro Suite 2017-1 Mutate Residue module (Schrödinger, LLC, New York, NY). The template structure of $APPI_{M17G/I18F/F34V}$ was the crystal structure of this protein in a complex with human mesotrypsin [Protein Data Bank (PDB) ID:

Downloaded from http://portlandpress.com/biochemj/article-pdf/475/7/1335/694517/bcj-2018-0070.pdf by Ben-Gurion University of the Negev user on 23 August 2021

© 2018 The Author(s). Published by Portland Press Limited on behalf of the Biochemical Society

Biochemical Journal (2018) **475** 1335–1352
https://doi.org/10.1042/BCJ20180070

PORTLAND PRESS

5C67]. The P13W mutation was performed on the mesotrypsin protein complex to avoid intermolecular clashes.

$APPI_{P13W/M17G/I18F/F34V}$ and $APPI_{M17G/I18F/F34V}$ were docked to human mesotrypsin and hK6 by using Discovery Studio 4.5 (Biovia, Dassault Systemes, San Diego, CA, U.S.A.) with ZDOCK, which is a rigid-body docking program that is based on fast Fourier transform correlation techniques and that searches all possible binding positions of the two proteins. The ZRANK method was used for quickly and accurately re-ranking the docked protein complexes predicted by ZDOCK. The ZRANK scoring function is a linear combination of van der Waals attractive and repulsive energies, short- and long-range repulsive and attractive energies, and desolvation [39]. The final top 2000 docking solution orientations were clustered into groups according to their spatial proximity by using an RMSD cutoff of 6 and an interface cutoff of 9 to assist in the selection for further analysis of the most promising docking solutions resembling the native protease–inhibitor interaction [40,41].

The proteins human mesotrypsin (5C67 and 3L33) and human hK6 (PDB ID: 5NX1) were prepared prior to docking using the Prepare Protein module, which can correct the enumeration of hydrogens by using standard pKa or predicted pK values, resulting in preferred hydrogen representation and protonation states of chain termini and side chains.

Results

The yeast-displayed triple-mutant $APPI_{M17G/I18F/F34V}$ binds unselectively to human serine proteases

In our recent study, we identified a triple-mutant $APPI_{M17G/I18F/F34V}$ that exhibited high proteolytic stability and high binding affinity to mesotrypsin [10], but lacked adequate specificity for *in vivo* preclinical studies [10]. To improve the binding specificity of the APPI triple mutant while preserving its superior affinity and stability for mesotrypsin — and thereby to identify second-generation highly selective APPI clones — in the current study, we used $APPI_{M17G/I18F/F34V}$ as the starting scaffold to generate a potent library for directed evolution (selective screens by YSD). To direct the evolutionary pressure on the APPI library for mesotrypsin specificity, we used human hK6 and human cationic and anionic trypsins as off-targets that bind tightly to APPI and therefore serve as competitors for *in vivo* mesotrypsin binding [10,42]. For the human trypsins, catalytically inactive S195A mutant enzymes were employed to eliminate the potential for autoproteolytic degradation and, in the case of mesotrypsin, to eliminate potential cleavage of APPI, thereby allowing us to exert a precise selection pressure for binding independent of proteolytic stability.

To test the ability of the yeast-displayed $APPI_{M17G/I18F/F34V}$ to detect and bind the enzymes unselectively, we first assembled the $APPI_{M17G/I18F/F34V}$ gene (and the APPI library, see below) using PCR and cloned it into the YSD vector (pCTCON) via transformation of EBY100 yeast cells. To enable us to perform binding titration experiments for each enzyme, the yeast cells were then induced for APPI protein expression by incubating yeast-displayed $APPI_{M17G/I18F/F34V}$ with different concentrations of the appropriate fluorescently labeled enzyme (0.1–1000 nM). After a washing step, the cells were monitored by flow cytometry for the detection of bound fluorescently labeled enzymes (Figure 1A). We found that the apparent affinities of the yeast-displayed APPI triple mutant for the different enzymes were similar (between 26 and 55 nM; Figure 1A), thus showing that the system was not selective.

To perform an unbiased competition assay in which the enzymes bind evenly to the yeast-displayed $APPI_{M17G/I18F/F34V}$, we determined the enzyme concentrations for which similar fluorescence signals for binding to each enzyme were observed (Figure 1A). As expected, using these enzyme concentrations for double staining of the yeast-displayed $APPI_{M17G/I18F/F34V}$ with mesotrypsin together with each enzyme competitor (separately), we were able to achieve similar enzyme-binding distributions, as detected by flow cytometry (Figure 1B).

Selective sorting of the APPI library

In light of the above results, we assumed that by conducting our binding competition assays with the 'unbiased' concentrations of the enzymes, which confer similar binding signals, we would be able to achieve uniform binding for simultaneous competition of the enzymes for the APPI library. It is known that APPI, being a member of the Kunitz family of inhibitors, is characterized by a canonical binding loop that determines the binding specificity [10,21,24,26] (Supplementary Figure S1). Thus, to increase our chances of improving

Downloaded from http://portlandpress.com/biochemj/article-pdf/475/7/1335/694517/bcj-2018-0070.pdf by Ben-Gurion University of the Negev user on 23 August 2021

© 2018 The Author(s). Published by Portland Press Limited on behalf of the Biochemical Society

Biochemical Journal (2018) **475** 1335–1352
https://doi.org/10.1042/BCJ20180070

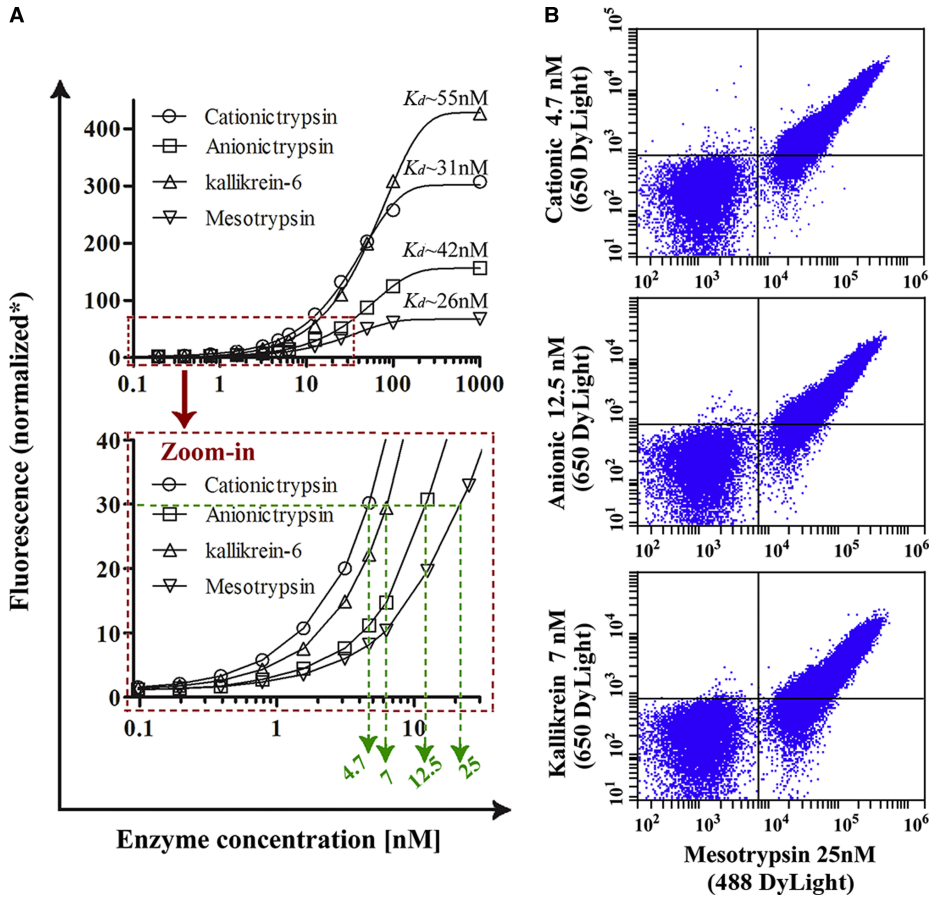

Figure 1. Determination of enzyme concentrations for selective maturation screenings.

(**A**) Binding titration curves of yeast-displayed $APPI_{M17G/I18F/F34V}$ with fluorescently labeled enzymes and corresponding K_d values are shown in the top panel. The zoom-in in the bottom panel was used to determine enzyme concentrations that produced similar binding signals (dashed green line). Calculated K_d values for cationic trypsin, anionic trypsin, hK6 and mesotrypsin were 31, 42, 55, and 26 nM, respectively. Data were analyzed using Prism, GraphPad Software, fitted to a one-site binding model. *Normalized fluorescence is the mean fluorescence value obtained by flow cytometry analysis normalized to the yeast autofluorescence. (**B**) Flow cytometry analysis of enzyme competition for the yeast-displayed $APPI_{M17G/I18F/F34V}$. Simultaneous competition reactions of mesotrypsin against cationic trypsin (top plot), anionic trypsin (middle plot) or hK6 (bottom plot) are shown. *X* and *Y* axes are fluorescence intensity signals of yeast-displayed APPI (represented by each point on the graph) for mesotrypsin binding (labeled with a DyLight 488 fluorophore) and competitor binding (labeled with a DyLight 650 fluorophore). Enzyme concentrations were as determined from (**A**) and are specified on each axis. Flow cytometry signals from each competition plot showed similar cell distributions and demonstrated an unbiased system at the enzyme concentrations used. Non-induced cells are located in the bottom left quadrant of each plot.

specificity using the combinatorial library, we focused the randomization mainly within the $APPI_{M17G/I18F/F34V}$ binding loop region (positions 11–18, excluding Cys at position 14; Supplementary Figure S1) using NNS degenerate codons (where N indicates A, C, G or T, while S represents G or C). Since we had recently shown that mutations that are in close proximity to the binding interface may also promote changes in the inhibitor affinity [10], additional mutations were introduced randomly throughout the whole APPI sequence to generate another level of diversity, especially around the inhibitor-/enzyme-binding site (Supplementary Figure S1). The frequency of mutations in the APPI library was 1–2 amino acids per clone, yielding an experimental library of 3.5×10^6 independent variants.

Our strategy to engineer mesotrypsin specificity in the APPI scaffold consisted of two steps (Figure 2A). First, a mixture of fluorescently labeled enzymes in unbiased concentrations was incubated with the yeast-

© 2018 The Author(s). Published by Portland Press Limited on behalf of the Biochemical Society

Downloaded from http://portlandpress.com/biochemj/article-pdf/475/7/1335/694517/bcj-2018-0070.pdf by Ben-Gurion University of the Negev user on 23 August 2021

Biochemical Journal (2018) **475** 1335–1352
https://doi.org/10.1042/BCJ20180070

displayed APPI library, and the enzymes were allowed to compete for binding. Second, unbound enzymes were washed out, and the bound cells exhibiting higher mesotrypsin binding were collected by FACS. In addition to using different enzymes, we increased the evolutionary pressure by using: (i) decreasing concentrations of mesotrypsin in successive sorting cycles and (ii) incubation times that were shorter than the expected or estimated times to achieve equilibrium binding based on solution studies (Supplementary Figure S4). It was thus evident that performing selection under pre-equilibrium conditions would facilitate the identification of the most selective APPI inhibitor with emphasis on improvement in the association rate constant.

Prior to specificity enrichment, the initial library (termed S_0) was sorted both for sequences that were in frame and for high APPI expression levels, based on C-terminal c-Myc epitope tag detection, using fluorescent labeling of anti-c-Myc and anti-Fc antibodies. The S_1 library so obtained (data not shown) was then subjected to four subsequent rounds of specificity maturation steps, each performed with unbiased concentrations of hK6, cationic trypsin and anionic trypsin, and decreasing concentrations of mesotrypsin (red columns in Figure 2B,C). The diffuse distribution of the fluorescence signals on both axes of the flow cytometry plot suggested that there was substantial heterogeneity in enzyme-binding specificity in the S_1 pool (Figure 2B). We thus used diagonal sorting gates to select cell populations having high-affinity levels for mesotrypsin but comparably lower affinity for the other enzymes (Figure 2B). This sorting strategy ensured that only those cells for

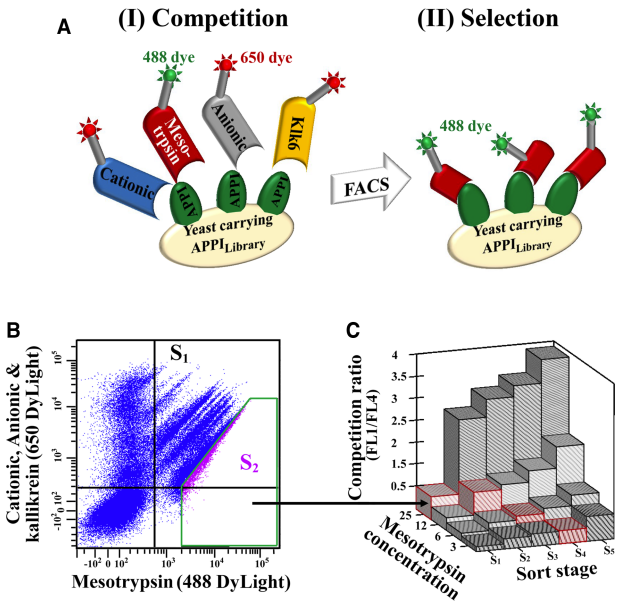

Figure 2. Selective maturation of yeast-displayed APPI.

The APPI library was sorted for preference for mesotrypsin binding over cationic trypsin, anionic trypsin and hK6. (**A**) General scheme of the selective maturation procedure: (I) fluorescently labeled mesotrypsin (488 fluorophore) and competitor enzymes (labeled with 650 fluorophore) were allowed to compete for APPI binding; (II) APPI clones that favored mesotrypsin binding were selected by FACS [e.g. as S_2 population in (**B**)]. (**B**) FACS of the initial selectivity sort (S_1). *X* and *Y* axes are fluorescence intensity signals of the yeast-displayed APPI library (represented by each point on the graph) (S_1) for mesotrypsin binding (labeled with a DyLight 488 fluorophore) and competitors binding (labeled with a DyLight 650 fluorophore), respectively. Fluorescence signals from the YSD APPI library showed several populations with high heterogeneity for enzyme binding, suggesting that APPI variants in the library had different enzyme specificities. Non-induced cells are located in the bottom left quadrant of each plot. A diagonal sorting gate (green) was used to select the S_2 population (having a high affinity to mesotrypsin but relatively low affinity to the other competitor enzymes). (**C**) 3D bar plot of mesotrypsin-/competitor-binding ratios obtained by flow cytometry analysis. Ratios of mesotrypsin binding relative to the competitor binding (competition ratio) are shown for sorting rounds S_1–S_5. Higher ratios indicate higher mesotrypsin binding relative to the binding of competitors. Concentrations of mesotrypsin were 25, 12, 6 and 3 nM for sorts S_1, S_2, S_3 and S_4, respectively. The concentrations of anionic trypsin, cationic trypsin and hK6 in all sorts were 12.5, 4.7 and 7 nM, respectively. Red columns indicate values obtained upon sorting.

© 2018 The Author(s). Published by Portland Press Limited on behalf of the Biochemical Society

Downloaded from http://portlandpress.com/biochemj/article-pdf/475/7/1335/694517/bcj-2018-0070.pdf by Ben-Gurion University of the Negev user on 23 August 2021

Biochemical Journal (2018) **475** 1335–1352
https://doi.org/10.1042/BCJ20180070

which mesotrypsin binding outcompeted binding to the competitor, as demonstrated by greater signal on the 488 Dylight channel compared with the 650 Dylight channel, would be captured and enriched. Flow cytometry analysis of mesotrypsin binding — in the presence of a mixture of enzyme competitors — to cell populations from the library maturation cycles (S_1 to S_5) showed that the more mature the sort, the higher the specificity (competition ratio) of the mutant library for mesotrypsin (Figure 2C). Remarkably, the S_5 pool showed high enhancement in mesotrypsin specificity, being ∼8× greater than that of the initial S_1 library at all mesotrypsin concentrations used (Figure 2C).

The P_3 residue in APPI is of substantial importance in mesotrypsin specificity

To identify yeast-displayed APPI clones with improved mesotrypsin specificity, we sequenced at least 20 different APPI clones after each round of sorting and analyzed their sequences (Supplementary Figure S2). Sequence analysis showed a broad distribution of nonrepeating multiple mutations (throughout the entire protein sequence, not only in the binding loop) in the early sorts, which converged to a few mutations with a high frequency in the later sorting stages, namely, six, five and two variants in sorts S_3, S_4 and S_5, respectively. Not surprisingly, most of the mutations were detected within the APPI-binding loop, notably with a marked preference for the inhibitor P_3 position. This finding suggests that the P_3 position in the APPI sequence plays a unique role in mesotrypsin specificity. Clones that were identified by sequencing of sorts S_3–S_5 were then analyzed by flow cytometry to estimate their specificity enhancement for mesotrypsin relative to clone $APPI_{M17G/I18F/F34V}$ (Figure 3). The results obtained from testing the affinity of the YSD individual clones for mesotrypsin and the other proteases confirmed that the APPI library was, for the most part, enriched for improvement in mesotrypsin specificity, but to different degrees.

We were aware that the specificity assessed using our YSD methodology may differ from that *in vivo* for two reasons: first, the APPI variants, being bound to the yeast, suffer from restricted solubility and mobility. Second, the enzymes are either chemically modified (fluorescently labeled) or unable to hydrolyze peptides (genetically mutated to form an inactive variant), which may affect their ability to bind APPI due to steric hindrance or to small structural changes. Thus, to assess enzyme specificity in a more accurate manner, we expressed and purified active forms of human mesotrypsin, cationic trypsin, anionic trypsin and hK6, and also the soluble forms of $APPI_{M17G/I18F/F34V}$ and the five other APPI mutants shown in Table 1, all of which showed improvements in mesotrypsin specificity, based on the YSD analysis. The soluble forms of the APPI

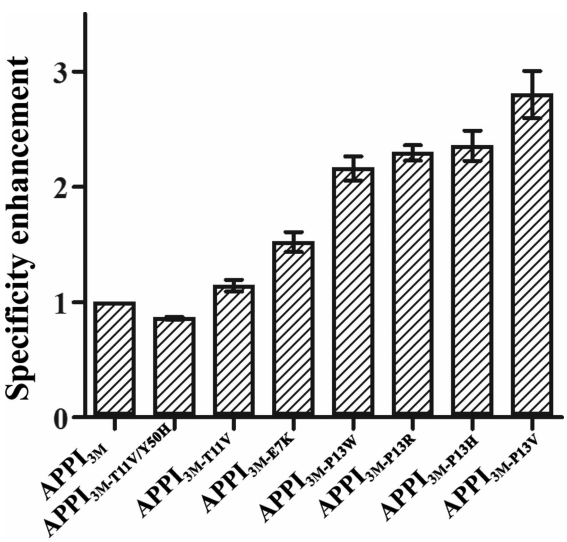

Figure 3. Selectivity-matured APPI variants show improved mesotrypsin specificity in the yeast surface display format.
The affinity of yeast-displayed APPI variants that had been sorted for mesotrypsin-binding specificity was determined by flow cytometry analysis for mesotrypsin (10 nM) relative to the competitor proteins (in concentrations of 12.5, 4.7 and 7 nM for anionic trypsin, cationic trypsin and hK6, respectively). Specificity enhancement is the value obtained relative to $APPI_{M17G/I18F/F34V}$; therefore, numbers greater than 1 indicate that specificity was improved. Results (means ± SD) were obtained from three independent experiments.

Downloaded from http://portlandpress.com/biochemj/article-pdf/475/7/1335/694517/bcj-2018-0070.pdf by Ben-Gurion University of the Negev user on 23 August 2021

© 2018 The Author(s). Published by Portland Press Limited on behalf of the Biochemical Society

Biochemical Journal (2018) **475** 1335–1352
https://doi.org/10.1042/BCJ20180070

Table 1 Specificity improvement of APPI quadruple variants for mesotrypsin inhibition versus the triple-mutant scaffold

	K_i^{eq} specificity			K_{off} specificity			K_{on} specificity			Total specificity[†]
	hK6	Cationic	Anionic	hK6	Cationic	Anionic	hK6*	Cationic	Anionic	
APPI_3Mut[‡]	1.0	1.0	1.0	1.0	1.0	1.0	1.0	1.0	1.0	1.0
APPI_3Mut$_{P13R}$	**2.3**	0.5	**2.0**	**1.5**	**1.2**	**2.0**	**1.7**	0.7	**1.2**	1.4
APPI_3Mut$_{P13H}$	**4.9**	0.6	**2.9**	**1.2**	0.6	**1.3**	**4.5**	**1.1**	**2.2**	1.8
APPI_3Mut$_{P13W}$	**29.9**	**1.2**	**2.4**	**3.8**	**1.1**	**1.7**	**8.3**	**1.4**	**2.1**	3.1
APPI_3Mut$_{P13V}$	**1.7**	0.5	**1.7**	0.8	0.9	**1.5**	**2.5**	0.6	**1.5**	1.3
APPI_3Mut$_{T11V}$	**1.6**	0.9	**2.5**	1.0	**1.1**	**2.1**	**1.6**	**1.1**	1.0	1.3

Bold numbers represent specificity improvements (numbers greater than 1).
*K_{on} specificity values for hK6 were calculated from K_{on}^{calc}.
[†]Total specificity is the average of K_{on} and K_{off} specificity improvement values in each row.
[‡]APPI_3Mut = APPI$_{M17G/I18F/F34V}$.

variants were obtained by cloning their sequences into a pPIC9K vector following transformation, expression (in *P. pastoris*) and purification, as described in our recent work [10]. We then obtained equilibrium (K_i) and kinetic (k_{on} and k_{off}) constants for each enzyme–inhibitor combination by conducting competitive inhibition experiments using a spectrophotometric assay to detect enzyme activity in the reaction mixture. In these assays, progress curves were generated by monitoring the cleavage of a competitive substrate (the chromogenic substrate for the trypsins was Z-GPR-pNA and the fluorogenic substrate for hK6 was BOC-FSR-AMC) by the appropriate enzyme in the presence of various concentrations of each inhibitor (Figure 4A,B). The data generated from the progress curves were used to calculate the affinity constants (i.e. K_i, k_{on} and k_{off}) using eqns (1–8) as described in *Materials and Methods* and Figure 4B–D (results are summarized in Supplementary Tables S2–S5). The affinity constants K_i, k_{on} and k_{off} (Supplementary Tables S2–S5) were then used to calculate improvements in APPI specificity to mesotrypsin relative to each enzyme by using eqns (9 and 10), which are given in the Materials and Methods section (Table 1).

Comparison of specificity values from the equilibrium inhibition constants (K_i) of APPI variants shows that for all APPI variants, the binding specificity for mesotrypsin was largely improved over hK6, only slightly improved over anionic trypsin and remained unchanged for cationic trypsin (Table 1). Nevertheless, in most cases, the APPI variants showed improved specificity in terms of the association constant (k_{on}) vis-à-vis cationic trypsin (Table 1). Additionally, specificity values from the association constant were improved in 80% of the cases (Table 1). A comparison of the total improvement in k_{on} specificity for all the variants (the average of k_{on} specificity values for any enzyme–inhibitor combination) with total improvement in k_{off} specificity shows that improvement in total k_{on} specificity was ∼1.5× greater than total k_{off} specificity, which validates our pre-equilibrium sorting strategy. Most importantly, we identified a quadruple mutant APPI variant, namely APPI$_{P13W/M17G/I18F/F34V}$, with improved mesotrypsin specificity values in all parameters (k_i, k_{on} and k_{off}) vis-à-vis all enzymes, with 3-fold improvement in total specificity compared with APPI$_{M17G/I18F/F34V}$ (Table 1). This mutant also showed the highest k_{on} value for mesotrypsin binding in comparison with the other APPI variants (Supplementary Table S2). Additionally, the k_{on} value of APPI$_{P13W/M17G/I18F/F34V}$ for mesotrypsin (8.0×10^6 M^{-1} s^{-1}) was greater than its k_{on} values for cationic trypsin (3.0×10^6 M^{-1} s^{-1}) and hK6 (4.0×10^5 M^{-1} s^{-1}), and comparable to that of anionic trypsin (9.6×10^6 M^{-1} s^{-1}) (Supplementary Tables S2–S5). These results are consistent with our pre-equilibrium sorting approach and the library sequencing analysis in which APPI$_{P13W/M17G/I18F/F34V}$ was found in 80% of the sequences of the last sort (S_5).

Since we had previously shown that the triple-mutant APPI$_{M17G/I18F/F34V}$ possessed improved proteolytic stability to mesotrypsin catalytic activity in comparison with wild-type APPI (APPI$_{WT}$) [10,27], in the current study we used it as a starting scaffold to generate a proteolytically resistant APPI library. Nevertheless, because the evolutionary pressure in our new screening strategy did not involve active enzymes (especially mesotrypsin), it was possible that the inherent resistance of the matured APPI variants could have been lost during the affinity maturation process. To verify that the proteolytic stability of our new APPI$_{P13W/M17G/I18F/F34V}$ mutant was indeed preserved, we evaluated its hydrolysis rate k_{cat} by using time course incubations with mesotrypsin in

Downloaded from http://portlandpress.com/biochemj/article-pdf/475/7/1335/694517/bcj-2018-0070.pdf by Ben-Gurion University of the Negev user on 23 August 2021

© 2018 The Author(s). Published by Portland Press Limited on behalf of the Biochemical Society

Biochemical Journal (2018) **475** 1335–1352
https://doi.org/10.1042/BCJ20180070

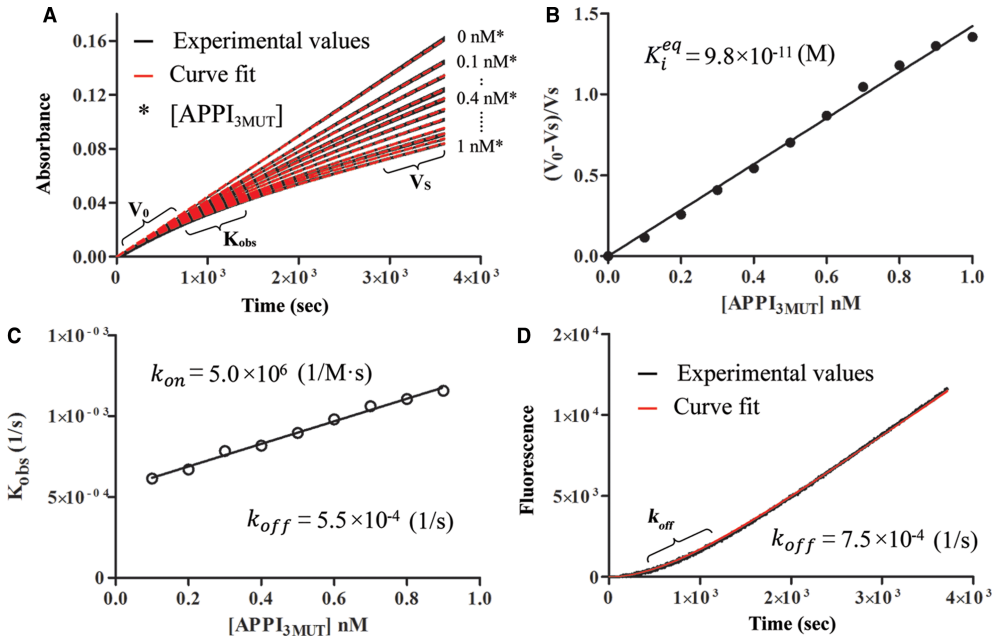

Figure 4. Kinetics of enzyme inhibition by APPI.

Representative examples of determination of the kinetic constants for enzyme inhibition by APPI. (**A**) Progress curves for the inhibition of mesotrypsin by $APPI_{M17G/I18F/F34V}$ (designated $APPI_{3MUT}$). Mesotrypsin cleavage of the peptide substrate Z-GPR-pNA was competitively inhibited by $APPI_{M17G/I18F/F34V}$. Experimental values are shown in black, with the curve-fit to eqn (2) shown as dashed red lines. $APPI_{M17G/I18F/F34V}$ concentrations are shown on the right. V_s and V_0 are the steady-state rates in the presence and absence of inhibitor, and k_{obs} is the observed first-order rate constant, which describes the transition from V_0 to V_s from which the kinetic constants were calculated. (**B**) Slow, tight binding inhibition of mesotrypsin by $APPI_{M17G/I18F/F34V}$. Values of the equilibrium inhibition constant (K_i^{eq}) were calculated from the steady-state portion of the progress curves in (**A**) using eqn (1). (**C**) Determination of kinetic constants (k_{on} and k_{off}) for mesotrypsin inhibition by $APPI_{M17G/I18F/F34V}$. A plot with linear dependence of k_{obs} on the inhibitor concentration [according to eqn (3)] facilitated the calculation of k_{on} and k_{off}. (**D**) Progress curves for hK6 inhibition by $APPI_{M17G/I18F/F34V}$. hK6 cleavage of the peptide substrate BOC-Phe–Ser–Arg-AMC was competitively inhibited by $APPI_{M17G/I18F/F34V}$. Experimental values are shown in black, with the curve-fit to eqn (7) shown as a dashed red line. k_{off} is the first-order off-rate constant, which describes the transition from complete inhibition to a steady-state rate of partial inhibition. Concentrations of enzymes, inhibitors and substrates and the reaction time for each inhibition experiment are summarized in Supplementary Table S1. Results are the averages of at least three independent experiments.

which the intact protein was monitored by HPLC, as described recently [10] (Supplementary Figure S5). Hydrolysis studies for the cleavage of $APPI_{P13W/M17G/I18F/F34V}$ by mesotrypsin showed that its proteolytic stability [$k_{cat} = (4.9 \pm 0.3) \times 10^{-4}$ s^{-1}] was comparable to that of $APPI_{M17G/I18F/F34V}$ [$k_{cat} = (4.3 \pm 0.3) \times 10^{-4}$ s^{-1}] [10], which confirmed the suitability of using the proteolytically stable triple mutant as a starting point for our second-generation library. In addition, since we had previously shown that the specificity of $APPI_{M17G/I18F/F34V}$ to mesotrypsin was superior by five orders of magnitude to the specificity to factor XIa (FXIa), the most important physiological target of APPI [43,44], in the current study we did not use FXIa as a competitor for directed evolution. Nevertheless, to confirm that the low specificity to FXIa was conserved in our new $APPI_{P13W/M17G/I18F/F34V}$ protein, we performed competitive inhibition experiments to measure the quadruple mutant's affinity to FXIa by using different concentrations of inhibitor and S-2366 as the substrate, as described in detail in Supplementary Materials and Methods (Table 2). To determine the full spectrum of $APPI_{P13W/M17G/I18F/F34V}$ specificity improvement, we evaluated the specificity improvements versus $APPI_{WT}$ for all enzymes according to eqn (10) (Table 2).

The results confirm that the low specificity of $APPI_{P13W/M17G/I18F/F34V}$ for FXIa was indeed preserved, thereby conferring a five-orders-of-magnitude specificity preference for mesotrypsin inhibition (Table 2). Also notable were the affinity switches of $APPI_{P13W/M17G/I18F/F34V}$ compared with $APPI_{M17G/I18F/F34V}$ that could be observed from the fold change in their affinities toward hK6 and anionic trypsin: the affinity of $APPI_{P13W/M17G/I18F/F34V}$

© 2018 The Author(s). Published by Portland Press Limited on behalf of the Biochemical Society

Downloaded from http://portlandpress.com/biochemj/article-pdf/475/7/1335/694517/bcj-2018-0070.pdf by Ben-Gurion University of the Negev user on 23 August 2021

Biochemical Journal (2018) **475** 1335–1352
https://doi.org/10.1042/BCJ20180070

Table 2 Binding specificity of APPI$_{P13W/M17G/I18F/F34V}$ toward a range of human serine proteases

	K_i (M)				
Inhibitor	**Mesotrypsin**	**Kallikrein-6**	**Cationic trypsin**	**Anionic trypsin**	**FXIa**
APPI-WT*	$(1.3 \pm 0.2) \times 10^{-7}$ †	$(1.6 \pm 0.1) \times 10^{-9}$	$(4.1 \pm 0.1) \times 10^{-12}$	$(1.1 \pm 0.1) \times 10^{-12}$	$(4.1 \pm 0.1) \times 10^{-10}$ †
APPI-3M*,‡	$(9.8 \pm 0.1) \times 10^{-11}$	$(3.6 \pm 0.1) \times 10^{-10}$	$(2.3 \pm 0.1) \times 10^{-11}$	$(2.3 \pm 0.1) \times 10^{-12}$	$(9.8 \pm 0.3) \times 10^{-8}$
APPI-4M*,§	$(6.9 \pm 0.1) \times 10^{-11}$	$(7.6 \pm 0.1) \times 10^{-9}$	$(1.9 \pm 0.1) \times 10^{-11}$	$(3.8 \pm 0.1) \times 10^{-12}$	$(5.0 \pm 0.1) \times 10^{-8}$
APPI-3M versus APPI-4M					
Fold change	1.4	0.047	1.2	0.6	1.9
Specificity	1	29.9	1.2	2.3	0.7
APPI-WT versus APPI-4M					
Fold change	1884	0.21	0.22	0.29	8.2×10^{-3}
Specificity	1	8950	8730	6510	229 760

*Values are means ± SD of at least three independent experiments.
†Affinity constants reported recently in ref. [10].
‡APPI$_{M17G/I18F/F34V}$.
§APPI$_{P13W/M17G/I18F/F34V}$.

for mesotrypsin was improved 1.4×, whereas the affinity of hK6 and anionic trypsin was reduced by ∼20× and ∼2×, respectively, versus APPI$_{M17G/I18F/F34V}$. When compared with the affinity of APPI$_{WT}$, the affinity of APPI$_{P13W/M17G/I18F/F34V}$ for mesotrypsin was improved 1900×, whereas affinities for hK6, cationic trypsin, anionic trypsin and FXIa were reduced by 5×, 5×, 3× and 120×, respectively. This affinity switch results in remarkable specificity shifts, ranging from 6 500-fold up to 230 000-fold improvement in mesotrypsin inhibition.

Docking analysis

To better understand the role played by the P13W mutation in APPI in mesotrypsin affinity and specificity, a series of molecular docking simulations were performed to predict the binding mode of APPI$_{M17G/I18F/F34V}$ (PDB ID: 5C67 [10]) and of the most specific APPI$_{P13W/M17G/I18F/F34V}$ variant with human mesotrypsin (PDB ID: 5C67 [10] and 3L33 [24]) and human hK6 (PDB ID: 5NX1), the two proteases that showed the largest differences in binding to APPI$_{P13W/M17G/I18F/F34V}$. An analysis of the molecular interactions within each modeled complex can be used to predict the role that the P13W mutation may play in the improvement of APPI$_{P13W/M17G/I18F/F34V}$ binding specificity (and affinity) for mesotrypsin relative to hK6, as described in Table 1 and Supplementary Tables S2–S5.

Molecular docking of the APPI$_{P13W/M17G/I18F/F34V}$ mutant with mesotrypsin revealed that compared with Pro-13, Trp-13 occupies a groove within the mesotrypsin-binding site and therefore better geometrical shape complementarity is gained by mutating Pro-13 to Trp-13 (Figure 5A). Additionally, the Trp-13 aromatic ring is predicted to form a new π-cation interaction with the ε-amino group of mesotrypsin Lys-175 and a new π–π interaction with mesotrypsin Trp-215, while APPI-Tyr-35 may form a π-cation interaction with Arg-96 of mesotrypsin (Figure 5B). The side chain of mesotrypsin Asp-97 is predicted to rotate away from APPI Trp-13 and toward mesotrypsin Arg-96, thereby avoiding electrostatic repulsion. These stabilizing interactions in the APPI$_{P13W/M17G/I18F/F34V}$/mesotrypsin complex are consistent with the better ZRANK score for docking APPI$_{P13W/M17G/I18F/F34V}$ (versus APPI$_{M17G/I18F/F34V}$) with mesotrypsin (−115.0 and −108.4, respectively). The ZRANK method was used here for accurately re-ranking the docked protein complexes predicted by ZDOCK (a rigid-body docking algorithm designed to predict the complex structures). Unlike ZDOCK, the ZRANK scoring function is a linear combination of van der Waals attractive and repulsive energies, short- and long-range repulsive and attractive energies, and desolvation [39], providing improved accuracy. The predicted APPI$_{P13W/M17G/I18F/F34V}$/mesotrypsin interaction described above supports the preference of mesotrypsin for binding to APPI$_{P13W/M17G/I18F/F34V}$ over APPI$_{M17G/I18F/F34V}$, as found by our experimental binding studies (Supplementary Table S2).

Inhibition studies showed that APPI$_{P13W/M17G/I18F/F34V}$ has a much stronger affinity for mesotrypsin than for hK6 (>100-fold; Supplementary Tables S2, S5 and S6). This observation is also supported by the docked

Downloaded from http://portlandpress.com/biochemj/article-pdf/475/7/1335/694517/bcj-2018-0070.pdf by Ben-Gurion University of the Negev user on 23 August 2021

© 2018 The Author(s). Published by Portland Press Limited on behalf of the Biochemical Society

Biochemical Journal (2018) **475** 1335–1352
https://doi.org/10.1042/BCJ20180070

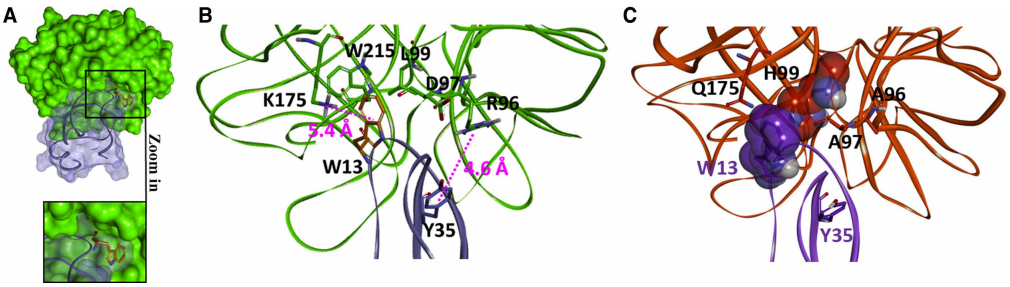

Figure 5. Docked models of APPI$_{P13W/M17G/I18F/F34V}$ complexed with human mesotrypsin and hK6.
(**A**) Mesotrypsin is depicted as a green surface and APPI as a purple ribbon, with Trp-13 shown by an orange stick representation. (**B**) Detail of predicted interactions between Trp-13 (orange) of APPI (purple) with mesotrypsin (green). APPI-Tyr-35 exhibits a potential π-cation interaction with Arg-96 of mesotrypsin, while APPI Trp-13 forms a similar interaction with mesotrypsin Lys-175. (**C**) Detail of predicted interactions between APPI Trp-13 and hK6. hK6 is represented by orange ribbons and APPI$_{P13W/M17G/I18F/F34V}$ is shown in purple. hK6 His-99 may potentially clash with APPI Trp-13 (residues shown by the space-filling model). hK6 residues Gln-175, Ala-96 and Ala-97 (shown by stick representations) do not form the potentially stabilizing interactions observed for the alternative residues found in these positions in mesotrypsin, as described in (**B**).

complex of hK6 with APPI$_{P13W/M17G/I18F/F34V}$, mainly by the loss of important interactions that stabilize the complex, as shown in Figure 5C. In addition to the possible clash of hK6 His-99 with APPI Trp-13, the electrostatic π-cation interaction, which is observed between APPI Trp-13 and mesotrypsin Lys-175, is not present in hK6 since Gln-175 (hK6) replaces the Lys-175 (in mesotrypsin) (Figure 5C). The destabilizing interactions in the APPI$_{P13W/M17G/I18F/F34V}$/ hK6 complex are consistent with the inferior ZRANK score for docking APPI$_{P13W/M17G/I18F/F34V}$ with hK6 and mesotrypsin (−95.4 and −115.0, respectively).

Overall, better affinity to mesotrypsin due to new favorable interactions (Figure 5B) and lower affinity to hK6 due to deleterious interactions (Figure 5C) may explain the specificity switch in APPI$_{P13W/M17G/I18F/F34V}$ (versus APPI$_{M17G/I18F/F34V}$) toward mesotrypsin inhibition (Table 2 and Supplementary Tables S2, S5 and S6); this result is the outcome of our selective screening strategy.

Discussion

In the present study, utilization of the YSD system, together with a novel pre-equilibrium, competitive screening strategy of an APPI library, enabled us to identify a combination of mutations in the APPI sequence that improves the association rate and binding specificity of APPI toward mesotrypsin in preference to other serine proteases. Evaluating the binding specificity of the identified APPI variants (by inhibition studies and flow cytometry analysis; Supplementary Tables S2–S5, Table 1 and Figure 3), together with sequencing analyses (Supplementary Figure S2), showed that residue 13, the P_3 position in the APPI-binding loop, is uniquely tolerant to mutation and can therefore be manipulated to enhance specificity. The use of degenerate codons, particularly at mutation-tolerant positions, allowed for the incorporation of multiple mutations in these positions that did indeed enhance specificity to different degrees. Our results suggest that APPI residue 13 can be considered as a binding 'cold spot,' i.e. a position exhibiting suboptimal interactions where mutation is likely to improve binding affinity, as others have recently proposed in various studies of protein–protein interactions [45]. An important novel finding here was that in our system, the mutation-tolerant position complied with the cold-spot definition but for specificity (selective binding to mesotrypsin) rather than for affinity (increased binding to mesotrypsin). As shown by our experimental findings, most of the selected mutations at the P_3 position did not exhibit improved mesotrypsin affinity (except one, namely, P13W, Supplementary Table S2). Nonetheless, all of them did improve mesotrypsin specificity, yielding an overall improvement that ranged from ∼1.3-fold to ∼3.1-fold, versus the other proteases (Table 1). These results are anticipated to derive directly from our specificity maturation approach.

The specificity improvement of our best quadruple mutant (namely, APPI$_{P13W/M17G/I18F/F34V}$) relative to the parental APPI$_{M17G/I18F/F34V}$ protein derives primarily from improvements in selectivity for mesotrypsin versus hK6 (∼30-fold). When comparing the APPI$_{P13W/M17G/I18F/F34V}$ quadruple mutant with APPI$_{WT}$, for which there were pre-existing differences in binding affinity between mesotrypsin and other serine proteases ranging

© 2018 The Author(s). Published by Portland Press Limited on behalf of the Biochemical Society

Downloaded from http://portlandpress.com/biochemj/article-pdf/475/7/1335/694517/bcj-2018-0070.pdf by Ben-Gurion University of the Negev user on 23 August 2021

PORTLAND PRESS

from 100-fold to 100 000-fold (in favor of the other proteases, Supplementary Table S6), the best quadruple mutant exhibited a significant affinity shift of 1900-fold for mesotrypsin and a reduced affinity (by 5- to 120-fold) for the other proteases (Table 2). The improvements in affinity to mesotrypsin but not to the other proteases conferred net specificity shifts on the quadruple mutant (relative to $APPI_{WT}$) ranging from 6500-fold to 230 000-fold versus the competitors tested. The best quadruple mutant obtained in the present work is therefore a more potent mesotrypsin binder than any other naturally occurring or experimentally designed inhibitor yet reported [10,21,24,26].

In addition to the improvement in the mesotrypsin K_i of our quadruple mutant relative to the other proteases, the association rate k_{on} of our quadruple mutant to mesotrypsin was also enhanced, while its association rates to the other proteases were reduced (Supplementary Tables S2–S5). The improvements in binding specificity of the quadruple mutant, in terms of both K_i and k_{on} values for mesotrypsin versus other proteases, may also provide improved specificity under *in vivo* conditions in which mesotrypsin is present together with other human serine proteases that can compete for binding to APPI.

Because we labeled both the target and the competitor enzymes, we were able to perform the selection strategy in such a way that, in each round of selection, we chose only those mutants that specifically bound mesotrypsin, i.e. mutants that exhibited both high affinity to mesotrypsin and a low preference for binding to the competitor proteases, and in essence this is the innovative design element in our set-up. For example, if, in each round, we had selected mutants that showed high binding for the target enzyme (mesotrypsin) in the presence of competitor enzymes that were not fluorescently labeled (as has been done previously, [46]), we may have obtained mutants that bind mesotrypsin with high affinity but also exhibit higher affinity for the other serine proteases.

Our selection strategy also aimed to improve the association rate k_{on} in light of the role played by the concentrations of the inhibitor and the protease in effective competition *in vivo*: since the time required to reach inhibitor–enzyme equilibrium is greater at low concentrations (as frequently occurs *in vivo*), we used short incubation times in which competition between targets takes place in the pre-equilibrium state. This selection under kinetic conditions is analogous to the rapid *in vivo* maturation of antibodies in the body for which both rapid and specific binding are essential [47]. Interestingly, this new methodology of pre-equilibrium library selection for selecting fast-associating protein complexes has also been used very recently by another group (unbeknown to us at the time) [48] for generating faster association of TEM1 β-lactamase proteins to their inhibitor protein BLIP, but our approach offers the additional advantage of screening for selectivity and for rapid association. Thus, our approach provides an innovative strategy for engineering other targets for which rapid and selective association is required.

Since previous site-directed mutagenesis approaches were able to assess only the effects of single mutations, studies using these approaches may have overlooked mutations at the binding interface that are enhanced solely in the presence of neighboring mutations. This problem is, to some degree, circumvented in the use of DNA libraries, since multiple mutations can be engineered at particular neighboring positions by means of rational mutagenesis or by random mutagenesis throughout the binding interface, followed by selection for those combinations of mutations that possess the desired effects. In the current work, we used a combination of two randomization techniques for generating a potent APPI library: the first strategy was a predesigned focused loop library with single mutations only at particular canonical binding loop positions on APPI, and the second strategy was a completely random library containing 1–2 mutations throughout the entire APPI sequence. Importantly, in the mesotrypsin selection, we obtained APPI mutations mostly in the binding loop. Mutants having a combination of mutations outside and inside the binding loop or mutants with mutations only outside the loop were also obtained but at very low frequencies (Supplementary Figure S2). These low-frequency mutants were not analyzed further, mostly because they exhibited low specificity in flow cytometry analyses (Figure 3) or because they were identified at the first sort stages and were therefore not fully matured (Supplementary Figure S2).

As noted above, APPI selection failed to identify potent mutations generated from the random library (mutations outside the binding loop). Many possible reasons can be proposed for this failure: first, it is very likely that the mutations within the binding loop, which are in closer contact with the enzyme, facilitate a more dominant interaction, thereby masking the interactions of mutations outside the binding loop. Second, sequencing of the library (prior to selection) revealed that most of the mutants — 75% — carry the mutation within the binding loop, with the remainder having an additional mutation outside the binding loop (data not shown). Third, for the error-prone PCR used for generation of our random library, there is a substantial likelihood that

Downloaded from http://portlandpress.com/biochemj/article-pdf/475/7/1335/694517/bcj-2018-0070.pdf by Ben-Gurion University of the Negev user on 23 August 2021

© 2018 The Author(s). Published by Portland Press Limited on behalf of the Biochemical Society

Biochemical Journal (2018) 475 1335–1352
https://doi.org/10.1042/BCJ20180070

mutations will be synonymous or that some amino acid mutations will be very rare, since they may require two or three nucleotide mutations in the same codon. Thus, the use of focused libraries — as opposed to random libraries — increases the chances of successful design, since the rational design of focused libraries facilitates the incorporation of mutations or positions that are known *a priori* to be beneficial.

Analysis of the libraries after sorting was limited by the number of sequences that could be obtained from single colonies. Nonetheless, we judged it to be unnecessary to sequence additional clones, because the library size had decreased significantly by the fourth round of selection in the case of the selective/competitive screens; further sequencing would probably not have identified greater mutational diversity at the final sorting stages.

Using computationally generated models of inhibitor/enzyme complexes, we were able to identify distinct patterns that appear to be important for APPI-binding specificity for mesotrypsin relative to hK6. Our analysis revealed that the replacement of Pro-13 with Trp in the P_3 position in the APPI sequence (P13W) probably facilitated improved steric interactions with mesotrypsin in that new favorable π-cation interactions between the ε-amino group of mesotrypsin Lys-175 and the indole aromatic ring of APPI Trp-13 were predicted. Similarly, the replacement of Pro with Trp at P13W probably introduced an electrostatic π-cation interaction between APPI Trp-13 and mesotrypsin Lys-175 but not between APPI and hK6, since hK6 has Gln but not Lys at position 175.

As potential contributors to the improved K_i and k_{on} of APPI_3Mut$_{P13W}$, we also identified a possible π–π interaction between W13 of APPI_3Mut$_{P13W}$ and W215 of mesotrypsin. Other substitutions of APPI Pro-13 were also able to improve k_{on} and affect K_i. We note that the second-most improved variant in terms of k_{on} for association with mesotrypsin was actually APPI_3Mut$_{P13H}$. We have examined by docking the expected interaction between APPI_3Mut$_{P13H}$ and mesotrypsin, and found that His can make some of the same interactions as the Trp (i.e. with Trp-215 and His-217 in mesotrypsin). Nevertheless, Lys-175 in mesotrypsin adopts a different rotamer, far from APPI_3MutP13H facing the solvent, which might plausibly contribute to the slightly slower binding of APPI_3Mut$_{P13H}$ mesotrypsin in comparison with APPI_3Mut$_{P13W}$.

In the future, the APPI mutants that preferentially bind human mesotrypsin could be further optimized by using site-specific saturated mutagenesis within the entire binding interface (binding loop and neighboring residues, Supplementary Figure S1), thereby taking advantage of the long-range allosteric effects of interface mutations that may have been missed in our randomization for the reasons mentioned above. In addition, we plan to test the engineered APPI variants for their ability to inhibit cancer progression in cell cultures and animal disease models, followed by further development as diagnostic and therapeutic tools. Furthermore, specificity against other serine proteases could be achieved in a similar way and, consequently, APPI dimers could be developed for stronger affinity or greater functionality by combining two different APPI variants, each exhibiting specificity for a different serine protease target.

In summary, for the design of rapidly associating, high-affinity, selective mesotrypsin inhibitors, we have established a methodology integrating a combination of focused and random combinatorial methods for library design and a YSD technique for selective/competitive library screening under pre-equilibrium conditions. Such a methodology can be applied for future design of other protease inhibitors. Therefore, this work can be a model for future design projects for which data are available regarding the effects of mutation on binding affinity. Such mutations can be successfully combined, as shown here, with the use of the YSD set-up to obtain mutants possessing additional desirable characteristics.

Abbreviations

APPI, amyloid β-protein precursor Kunitz protease inhibitor domain; BGU, Ben-Gurion University of the Negev; BSA, bovine serum albumin; FACS, fluorescence-activated cell sorting; FXia, factor XIa; hK6, kallikrein-6; IKI, Ilse Katz Institute for Nanoscale Science and Technology; KB, kallikrein buffer; PDB, Protein Data Bank; TB, trypsin buffer; YSD, yeast surface display.

Author Contribution

I.C., S.N. and N.P. designed the research. I.C., S.N., A.H. and E.S.R. generated the proteins. I.C. and S.N. performed the research. I.C., S.N., E.B.Z. and N.P. analyzed the data. I.C. and N.P. wrote the paper. All authors edited the manuscript and approved the final version.

Funding

This work was supported by the European Research Council 'Ideas program' ERC-2013-StG (contract grant no. 336041) and the Prostate Cancer Foundation (PCF) to N.P., the DKFZ-MOST (contract grant no. GR2495) to N.P.

© 2018 The Author(s). Published by Portland Press Limited on behalf of the Biochemical Society

Downloaded from http://portlandpress.com/biochemj/article-pdf/475/7/1335/694517/bcj-2018-0070.pdf by Ben-Gurion University of the Negev user on 23 August 2021

N.P. and E.S.R. acknowledge support from the US-Israel Binational Science Foundation (BSF). E.S.R. acknowledges support from United Stated National Institutes of Health grant R01CA154387.

Acknowledgements

The authors thank Dr Alon Zilka and Dr Uzi Hadad for their technical assistance. FACS experiments were performed at the Ilse Katz Institute for Nanoscale Science and Technology, BGU.

Competing Interests

The Authors declare that there are no competing interests associated with the manuscript.

References

1 Koblinski, J.E., Ahram, M. and Sloane, B.F. (2000) Unraveling the role of proteases in cancer. *Clin. Chim. Acta* **291**, 113–135 https://doi.org/10.1016/S0009-8981(99)00224-7
2 Egeblad, M. and Werb, Z. (2002) New functions for the matrix metalloproteinases in cancer progression. *Nat. Rev. Cancer* **2**, 161–174 https://doi.org/10.1038/nrc745
3 Radisky, E.S. and Radisky, D.C. (2007) Stromal induction of breast cancer: inflammation and invasion. *Rev. Endocr. Metab. Disord.* **8**, 279–287 https://doi.org/10.1007/s11154-007-9037-1
4 Cudic, M. and Fields, G.B. (2009) Extracellular proteases as targets for drug development. *Curr. Protein Pept. Sci.* **10**, 297–307 https://doi.org/10.2174/138920309788922207
5 Turk, B. (2006) Targeting proteases: successes, failures and future prospects. *Nat. Rev. Drug Discov.* **5**, 785–799 https://doi.org/10.1038/nrd2092
6 Carter, P.J. (2006) Potent antibody therapeutics by design. *Nat. Rev. Immunol.* **6**, 343–357 https://doi.org/10.1038/nri1837
7 Adams, G.P. and Weiner, L.M. (2005) Monoclonal antibody therapy of cancer. *Nat. Biotechnol.* **23**, 1147–1157 https://doi.org/10.1038/nbt1137
8 López-Otín, C. and Matrisian, L.M. (2007) Emerging roles of proteases in tumour suppression. *Nat. Rev. Cancer* **7**, 800–808 https://doi.org/10.1038/nrc2228
9 de Witte, W.E.A., Vauquelin, G., van der Graaf, P.H. and de Lange, E.C.M. (2017) The influence of drug distribution and drug-target binding on target occupancy: the rate-limiting step approximation. *Eur. J. Pharm. Sci.* **109**, S83–S89 https://doi.org/10.1016/j.ejps.2017.05.024
10 Cohen, I., Kayode, O., Hockla, A., Sankaran, B., Radisky, D.C., Radisky, E.S. et al. (2016) Combinatorial protein engineering of proteolytically resistant mesotrypsin inhibitors as candidates for cancer therapy. *Biochem. J.* **473**, 1329–1341 https://doi.org/10.1042/BJ20151410
11 Rinderknecht, H., Renner, I.G., Abramson, S.B. and Carmack, C. (1984) Mesotrypsin: a new inhibitor-resistant protease from a zymogen in human pancreatic tissue and fluid. *Gastroenterology* **86**, 681–692 PMID:6698368
12 Diederichs, S., Bulk, E., Steffen, B., Ji, P., Tickenbrock, L., Lang, K., et al. (2004) S100 family members and trypsinogens are predictors of distant metastasis and survival in early-stage non-small cell lung cancer. *Cancer Res.* **64**, 5564–5569 https://doi.org/10.1158/0008-5472.CAN-04-2004
13 Hockla, A., Miller, E., Salameh, M.A., Copland, J.A., Radisky, D.C. and Radisky, E.S. (2012) PRSS3/mesotrypsin is a therapeutic target for metastatic prostate cancer. *Mol. Cancer Res.* **10**, 1555–1566 https://doi.org/10.1158/1541-7786.MCR-12-0314
14 Hockla, A., Radisky, D.C. and Radisky, E.S. (2010) Mesotrypsin promotes malignant growth of breast cancer cells through shedding of CD109. *Breast Cancer Res. Treat.* **124**, 27–38 https://doi.org/10.1007/s10549-009-0699-0
15 Jiang, G., Cao, F., Ren, G., Gao, D., Bhakta, V., Zhang, Y., et al. (2010) PRSS3 promotes tumour growth and metastasis of human pancreatic cancer. *Gut* **59**, 1535–1544 https://doi.org/10.1136/gut.2009.200105
16 Katona, G., Berglund, G.I., Hajdu, J., Gráf, L. and Szilágyi, L. (2002) Crystal structure reveals basis for the inhibitor resistance of human brain trypsin. *J. Mol. Biol.* **315**, 1209–1218 https://doi.org/10.1006/jmbi.2001.5305
17 Nyaruhucha, C.N., Kito, M. and Fukuoka, S.I. (1997) Identification and expression of the cDNA-encoding human mesotrypsin(ogen), an isoform of trypsin with inhibitor resistance. *J. Biol. Chem.* **272**, 10573–10578 PMID:9099703
18 Szmola, R., Kukor, Z. and Sahin-Tóth, M. (2003) Human mesotrypsin is a unique digestive protease specialized for the degradation of trypsin inhibitors. *J. Biol. Chem.* **278**, 48580–48589 https://doi.org/10.1074/jbc.M310301200
19 Salameh, M.A., Soares, A.S., Hockla, A. and Radisky, E.S. (2008) Structural basis for accelerated cleavage of bovine pancreatic trypsin inhibitor (BPTI) by human mesotrypsin. *J. Biol. Chem.* **283**, 4115–4123 https://doi.org/10.1074/jbc.M708268200
20 Salameh, M.A., Robinson, J.L., Navaneetham, D., Sinha, D., Madden, B.J., Walsh, P.N. et al. (2010) The amyloid precursor protein/protease nexin 2 Kunitz inhibitor domain is a highly specific substrate of mesotrypsin. *J. Biol. Chem.* **285**, 1939–1949 https://doi.org/10.1074/jbc.M109.057216
21 Pendlebury, D., Wang, R., Henin, R.D., Hockla, A., Soares, A.S., Madden, B.J. et al. (2014) Sequence and conformational specificity in substrate recognition: several human Kunitz protease inhibitor domains are specific substrates of mesotrypsin. *J. Biol. Chem.* **289**, 32783–32797 https://doi.org/10.1074/jbc.M114.609560
22 Alloy, A.P., Kayode, O., Wang, R., Hockla, A., Soares, A.S. and Radisky, E.S. (2015) Mesotrypsin has evolved four unique residues to cleave trypsin inhibitors as substrates. *J. Biol. Chem.* **290**, 21523–21535 https://doi.org/10.1074/jbc.M115.662429
23 Salameh, M.A., Soares, A.S., Alloy, A. and Radisky, E.S. (2012) Presence versus absence of hydrogen bond donor Tyr-39 influences interactions of cationic trypsin and mesotrypsin with protein protease inhibitors. *Protein Sci.* **21**, 1103–1112 https://doi.org/10.1002/pro.2097
24 Salameh, M.A., Soares, A.S., Navaneetham, D., Sinha, D., Walsh, P.N. and Radisky, E.S. (2010) Determinants of affinity and proteolytic stability in interactions of Kunitz family protease inhibitors with mesotrypsin. *J. Biol. Chem.* **285**, 36884–36896 https://doi.org/10.1074/jbc.M110.171348
25 Dennis, M.S., Herzka, A. and Lazarus, R.A. (1995) Potent and selective Kunitz domain inhibitors of plasma kallikrein designed by phage display. *J. Biol. Chem.* **270**, 25411–25417 https://doi.org/10.1074/jbc.270.43.25411
26 Salameh, M.A., Soares, A.S., Hockla, A., Radisky, D.C. and Radisky, E.S. (2011) The P_2' residue is a key determinant of mesotrypsin specificity: engineering a high-affinity inhibitor with anticancer activity. *Biochem. J.* **440**, 95–105 https://doi.org/10.1042/BJ20110788

Downloaded from http://portlandpress.com/biochemj/article-pdf/475/7/1335/694517/bcj-2018-0070.pdf by Ben-Gurion University of the Negev user on 23 August 2021

© 2018 The Author(s). Published by Portland Press Limited on behalf of the Biochemical Society

Biochemical Journal (2018) **475** 1335–1352
https://doi.org/10.1042/BCJ20180070

27 Kayode, O., Wang, R., Pendlebury, D.F., Cohen, I., Henin, R.D., Hockla, A. et al. (2016) An acrobatic substrate metamorphosis reveals a requirement for substrate conformational dynamics in trypsin proteolysis. *J. Biol. Chem.* **291**, 26304–26319 https://doi.org/10.1074/jbc.M116.758417

28 Boder, E.T., Midelfort, K.S. and Wittrup, K.D. (2000) Directed evolution of antibody fragments with monovalent femtomolar antigen-binding affinity. *Proc. Natl Acad. Sci. U.S.A.* **97**, 10701–10705 https://doi.org/10.1073/pnas.170297297

29 Boder, E.T. and Wittrup, K.D. (1997) Yeast surface display for screening combinatorial polypeptide libraries. *Nat. Biotechnol.* **15**, 553–557 https://doi.org/10.1038/nbt0697-553

30 Graff, C.P., Chester, K., Begent, R. and Wittrup, K.D. (2004) Directed evolution of an anti-carcinoembryonic antigen scFv with a 4-day monovalent dissociation half-time at 37°C. *Protein Eng. Des. Sel.* **17**, 293–304 https://doi.org/10.1093/protein/gzh038

31 Kieke, M.C., Shusta, E.V., Boder, E.T., Teyton, L., Wittrup, K.D. and Kranz, D.M. (1999) Selection of functional T cell receptor mutants from a yeast surface-display library. *Proc. Natl Acad. Sci. U.S.A.* **96**, 5651–5656 https://doi.org/10.1073/pnas.96.10.5651

32 Kim, Y.-S., Bhandari, R., Cochran, J.R., Kuriyan, J. and Wittrup, K.D. (2006) Directed evolution of the epidermal growth factor receptor extracellular domain for expression in yeast. *Proteins: Struct., Funct., Bioinf.* **62**, 1026–1035 https://doi.org/10.1002/prot.20618

33 Shusta, E.V., Holler, P.D., Kieke, M.C., Kranz, D.M. and Wittrup, K.D. (2000) Directed evolution of a stable scaffold for T-cell receptor engineering. *Nat. Biotechnol.* **18**, 754–759 https://doi.org/10.1038/77325

34 Chao, G., Lau, W.L., Hackel, B.J., Sazinsky, S.L., Lippow, S.M. and Wittrup, K.D. (2006) Isolating and engineering human antibodies using yeast surface display. *Nat. Protoc.* **1**, 755–768 https://doi.org/10.1038/nprot.2006.94

35 Chase, Jr, T. and Shaw, E. (1967) p-Nitrophenyl-p′-guanidinobenzoate HCl: a new active site titrant for trypsin. *Biochem. Biophys. Res. Commun.* **29**, 508–514 https://doi.org/10.1016/0006-291X(67)90513-X

36 Stein, R.L. (2011) *Kinetics of Enzyme Action: Essential Principles for Drug Hunters*, pp. 115–140. Wiley

37 Quast, U., Engel, J., Steffen, E., Tschesche, H. and Kupfer, S. (1978) Kinetics of the interaction of alpha-chymotrypsin with trypsin kallikrein inhibitor (Kunitz) in which the reactive-site peptide bond Lys-15-Ala-16 is split. *Eur. J. Biochem.* **86**, 353–360 https://doi.org/10.1111/j.1432-1033.1978.tb12317.x

38 Laskowski, Jr, M. and Kato, I. (1980) Protein inhibitors of proteinases. *Annu. Rev. Biochem.* **49**, 593–626 https://doi.org/10.1146/annurev.bi.49.070180.003113

39 Pierce, B. and Weng, Z. (2007) ZRANK: reranking protein docking predictions with an optimized energy function. *Proteins: Struct., Funct., Bioinf.* **67**, 1078–1086 https://doi.org/10.1002/prot.21373

40 Comeau, S.R., Gatchell, D.W., Vajda, S. and Camacho, C.J. (2004) Cluspro: an automated docking and discrimination method for the prediction of protein complexes. *Bioinformatics* **20**, 45–50 https://doi.org/10.1093/bioinformatics/btg371

41 Lorenzen, S. and Zhang, Y. (2007) Identification of near-native structures by clustering protein docking conformations. *Proteins: Struct., Funct., Bioinf.* **68**, 187–194 https://doi.org/10.1002/prot.21442

42 Navaneetham, D., Sinha, D. and Walsh, P.N. (2010) Mechanisms and specificity of factor Xla and trypsin inhibition by protease nexin 2 and basic pancreatic trypsin inhibitor. *J. Biochem.* **148**, 467–479 https://doi.org/10.1093/jb/mvq080

43 Badellino, K.O. and Walsh, P.N. (2000) Protease nexin II interactions with coagulation factor Xla are contained within the Kunitz protease inhibitor domain of protease nexin II and the factor Xla catalytic domain. *Biochemistry* **39**, 4769–4777 https://doi.org/10.1021/bi9925468

44 Navaneetham, D., Jin, L., Pandey, P., Strickler, J.E., Babine, R.E., Abdel-Meguid, S.S. et al. (2005) Structural and mutational analyses of the molecular interactions between the catalytic domain of factor Xla and the Kunitz protease inhibitor domain of protease nexin 2. *J. Biol. Chem.* **280**, 36165–36175 https://doi.org/10.1074/jbc.M504990200

45 Shirian, J., Sharabi, O. and Shifman, J.M. (2016) Cold spots in protein binding. *Trends Biochem. Sci.* **41**, 739–745 https://doi.org/10.1016/j.tibs.2016.07.002

46 Sarkar, C.A., Dodevski, I., Kenig, M., Dudli, S., Mohr, A., Hermans, E. et al. (2008) Directed evolution of a G protein-coupled receptor for expression, stability, and binding selectivity. *Proc. Natl Acad. Sci. U.S.A.* **105**, 14808–14813 https://doi.org/10.1073/pnas.0803103105

47 Foote, J. and Milstein, C. (1991) Kinetic maturation of an immune response. *Nature* **352**, 530–532 https://doi.org/10.1038/352530a0

48 Cohen-Khait, R. and Schreiber, G. (2016) Low-stringency selection of TEM1 for BLIP shows interface plasticity and selection for faster binders. *Proc. Natl Acad. Sci. U.S.A.* **113**, 14982–14987 https://doi.org/10.1073/pnas.1613122113

Downloaded from http://portlandpress.com/biochemj/article-pdf/475/7/1335/694517/bcj-2018-0070.pdf by Ben-Gurion University of the Negev user on 23 August 2021

© 2018 The Author(s). Published by Portland Press Limited on behalf of the Biochemical Society